Solvent resonance effect on the anisotropy of $NO^-(N_2O)_n$ cluster anion photodetachment

Luis Velarde, Terefe Habteyes, Emily R. Grumbling, Kostyantyn Pichugin, and Andrei Sanov[a)]
Department of Chemistry, University of Arizona, Tucson, Arizona 85721-0041, USA

(Received 14 June 2007; accepted 3 July 2007; published online 22 August 2007)

Photodetachment from $NO^-(N_2O)_n$ cluster anions ($n \leqslant 7$) is investigated using photoelectron imaging at 786, 532, and 355 nm. Compared to unsolvated NO^-, the photoelectron anisotropy with respect to the laser polarization direction diminishes drastically in the presence of the N_2O solvent, especially in the 355 nm data. In contrast, a less significant anisotropy loss is observed for $NO^-(H_2O)_n$. The effect is attributed to photoelectron scattering on the solvent, which in the N_2O case is mediated by the $^2\Pi$ anionic resonance. No anionic resonances exist for H_2O in the applicable photoelectron energy range, in line with the observed difference between the photoelectron images obtained with the two solvents. The momentum-transfer cross section, rather than the total scattering cross section, is argued to be an appropriate physical parameter predicting the solvent effects on the photoelectron angular distributions in these cluster anions. © *2007 American Institute of Physics*. [DOI: 10.1063/1.2766948]

I. INTRODUCTION

Studies of negatively charged clusters provide molecular-level views of chemical interactions relevant to anions in condensed environments.[1,2] Recent advances in photoelectron imaging[3–5] have renewed interest in solvation effects on cluster anion photodetachment, emphasizing the photoelectron angular distributions (PADs) measured simultaneously with the photoelectron spectra. Disappointingly, however, it is becoming a rather prevailing view that despite some notable exceptions[6] the PADs merely tend to become more isotropic with increasing cluster size. This leads to a perception that the information content of photoelectron images is limited for larger clusters.

To counter this perception, consider the loss of photodetachment anisotropy when the departing electron's kinetic energy (eKE) falls within the range of anionic resonances associated with the solvent network. As a general explanation, a resonance temporarily captures the photodetached electron before it is released into the continuum, scrambling its phase and angular momentum. Considering the complex electronic structures and aggregate properties of many solvents, it is not surprising that the solvent-induced, scattering-mediated loss of photoelectron anisotropy is a frequent occurrence in cluster chemistry. The diminished anisotropy, therefore, illuminates the role of photoelectron scattering on the solvent, complementing the information commonly derived from electron attachment and scattering spectra.[7]

For example, the photodetachment of the $I^-\cdot CH_3I$ cluster anion at 267 nm yields a PAD with a markedly low anisotropy magnitude, compared to other monosolvated iodide species, such as $I^-\cdot Ar$, $I^-\cdot H_2O$, and $I^-\cdot CH_3CN$.[8] The anisotropy loss has been attributed, among other possibilities, to scattering of the departing electron by the CH_3I solvent molecule. This mechanism has been argued on the basis of the high scattering cross section associated with a CH_3I^- shape resonance found close to the detached electron energy. More recently, Nakanishi *et al.* observed a similar effect in the detachment of acetone (Acn) cluster anions, $(Acn)_n^-$, where the PADs are found to be nearly isotropic for $n \geqslant 5$.[9] Analogous to the $I^-\cdot CH_3I$ case, the acetone molecules possess an anionic resonance in the photoelectron energy range.

In this paper, we discuss the solvent-induced photoelectron anisotropy effects in the photodetachment of the $NO^-(N_2O)_n$ cluster anions, with n ranging from 0 up to 7, depending on the laser wavelength. The photodetachment of some of these clusters has been studied previously without angular resolution, using traditional photoelectron spectroscopy[10,11] and photofragment-photoelectron coincidence techniques.[12] Unsolvated NO^- is adiabatically stable with respect to autodetachment only in its ground vibrational state.[13,14] Although it is an important anion in itself, the main focus of the present work is on the solvent role in electron photoemission from the NO^- cluster core. As the photoelectrons with specific eKE profiles propagate across the N_2O solvent shell, both elastic and inelastic scattering could, in general, lead to the reduction in the PAD anisotropy. It is expected that large-angle scattering, contributing the most to the momentum-transfer cross section,[15] should have the greatest effect on the measured PADs.

Previous electron scattering studies of N_2O are extensive (see, for example, Refs. 16 and 17 and references therein) providing evidence for two shape resonances in the low-eKE range: a Π symmetry resonance around 2.4 eV and a Σ resonance around 8 eV.[18] Vibrational Feshbach resonances near zero eKE have also been observed.[19,20] In the present work, the photoelectron imaging results for $NO^-(N_2O)_n$ are reported alongside the corresponding $NO^-(H_2O)_n$ data, high-

[a)]Electronic mail: sanov@u.arizona.edu

lighting the differences between the N_2O and H_2O solvents in their effects on the photodetachment anisotropies of the respective cluster anions.

II. EXPERIMENT

The experiments are performed on a negative-ion spectrometer described in detail elsewhere.[21] The instrument employs the ion techniques of Johnson and Lineberger,[22] combined with velocity-mapped[4] imaging[3] detection of photoelectrons. The cluster anions of interest are prepared starting with a pulsed supersonic expansion of a 20%–50% N_2O/Ar mixture into vacuum, with water contamination within the gas delivery lines as the source of H_2O. Anions are formed by secondary electron attachment to neutrals after ionizing the supersonic expansion with a 1 keV electron gun. The core NO^- anions are formed via the $N_2O+e^-\rightarrow O^-+N_2$, $O^-+N_2O\rightarrow NO^-+NO$ reaction sequence.[23,24]

The resultant anions are pulse extracted into a mass-spectrometer flight tube, at the end of which the ions of selected mass are intercepted with a linearly polarized laser pulse. Pulses of 786 nm (100 fs, <1 mJ) are derived from a Ti:sapphire laser system (Spectra Physics, Inc.). The harmonics of a nanosecond neodymium-doped yttrium aluminum garnet laser (Spectra Physics, Inc., Quanta-Ray Lab 130-50) provide 532, 355, and 266 nm pulses (approximately 30, 20, and 10 mJ/pulse, respectively). The photoelectrons are projected on a 40 mm diameter imaging detector (Burle, Inc.) in the direction perpendicular to the ion and laser beams. In all cases, the laser polarization direction is set parallel to the imaging detector plane. To discriminate against background, the detector is pulsed on for a 200 ns window coinciding with the arrival of the photoelectrons. The photoelectron images are recorded by a computer-controlled charge coupled device camera for $(1-5)\times10^4$ experimental cycles. The known vibrational lines of the bare NO^- photoelectron spectrum[25,26] are used for energy calibration. The PADs are analyzed using the basis set expansion (BASEX) program obtained from Dribinski *et al.*[27]

III. RESULTS AND ANALYSIS

A. Photoelectron images and energy spectra

Figure 1 shows the raw and Abel-inverted photoelectron images of unsolvated NO^-, collected at 786, 532, and 355 nm, along with the corresponding eKE spectra. The perceptible rings in the images correspond to the well-characterized[10,23,25,26] progression of transitions to the $X\,^2\Pi$, $v'=0-5$ vibrational states of NO from the ground $X\,^3\Sigma^-$, $v''=0$ state of NO^-. The rings appear congested at 355 nm, but the vibrational structure remains resolved, as emphasized in the magnified part of the image in Fig. 1(c). The outermost rings in all images correspond to the $0\leftarrow0$ transition, peaking at an electron binding energy (eBE$=h\nu-$eKE) of 0.04 ± 0.01 eV. Subject to rotational and spin-orbit corrections, this determination is consistent with the literature value of 0.026 ± 0.005 eV for the adiabatic electron affinity of NO.[25]

Figure 2 shows the 355 nm photoelectron images and the corresponding spectra for the $NO^-(N_2O)_n$, $n=0-5$ cluster anions. In addition to the data shown, the photoelectron images obtained at 355 nm for n up to 7, at 532 nm for $n=0-5$, and at 786 nm for $n=0-3$ are included in the foregoing analysis.[28] With the exception of the low-eKE spectral regions (discussed below), the energetic characteristics of the $NO^-(N_2O)_n$ photoelectron spectra in Fig. 2 are consistent with the electrostatically bound ion-neutral complexes studied previously by Bowen and co-workers,[10,11] where the excess electron is localized on the nitric oxide component of the cluster. The addition of each solvent N_2O molecule causes a spectral shift of about 0.2 eV to lower eKEs, accompanied by progressive broadening of the image rings and spectral peaks.

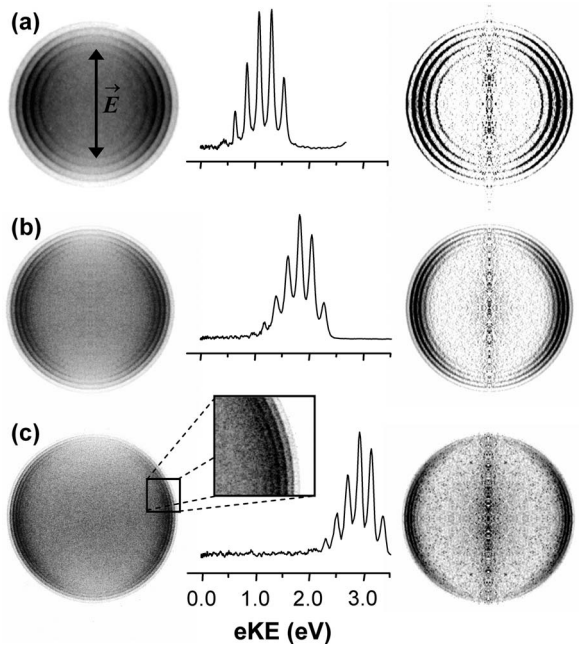

FIG. 1. Raw (left column) and Abel-inverted (right column) NO^- photoelectron images and the corresponding photoelectron spectra obtained at (a) 786 nm, (b) 532 nm, and (c) 355 nm. The images were taken under different electrostatic focusing conditions and are shown not to scale. Double arrow in (a) indicates the direction of the laser polarization for all images. Inset in (c) shows a magnified portion of the corresponding image.

The $NO^-(N_2O)_n$, $n=1$ image includes a central feature corresponding to slow photoelectrons. This feature is absent for unsolvated NO^- (Figs. 1 and 2, $n=0$) and nearly unobservable for $NO^-(N_2O)_n$, $n>1$ (Fig. 2). It is attributed to the covalent, w-shaped $N_3O_2^-$ singlet anion, as proposed by Hiraoka *et al.*[29] and characterized by Resat *et al.*[12] and Torchia *et al.*[30] Further confirmation of the presence of the $N_3O_2^-$ isomer in our experiment comes from a small N_2O^- photofragment signal, which we observed with our secondary reflectron mass spectrometer[31] in 532 nm dissociation of the $NO^-(N_2O)_n$, $n=1$ cluster.[28] As suggested by Snis and Panas,[32] this photofragment arises from a dissociative excitation of the covalent $N_3O_2^-$ anion. We excluded the low-eKE spectral regions from the anisotropy analysis, which was thus limited to the bands arising from the NO^- cluster core only.

Figure 3 shows 355 nm photoelectron images and the corresponding spectra of $NO^-(H_2O)_n$, $n=0-3$. The spectra are in agreement with the previous measurements by Eaton *et al.*[33] The loss of vibrational structure in the $NO^-(H_2O)_n$

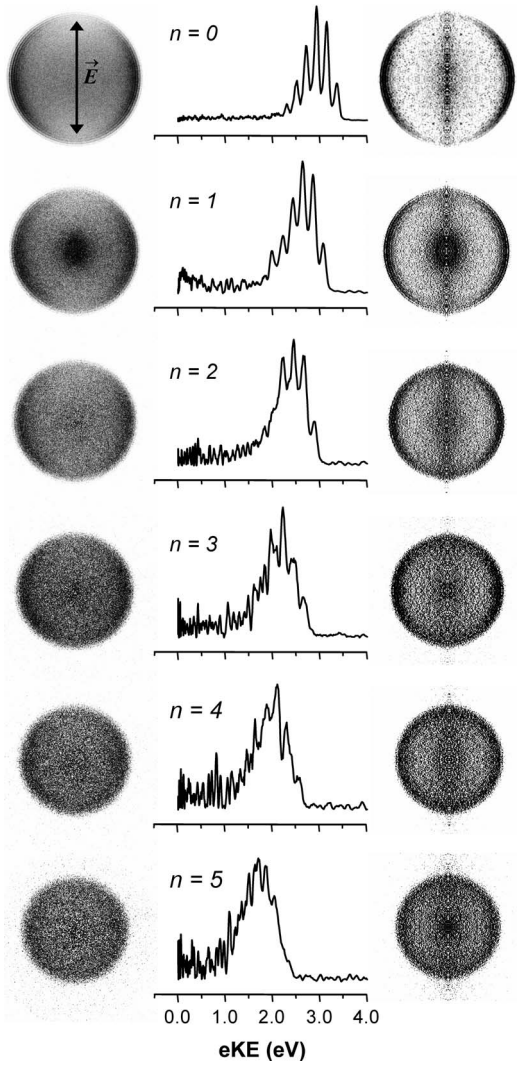

FIG. 2. Raw (left column) and Abel-inverted (right column) photoelectron images and the corresponding photoelectron spectra of $NO^-(N_2O)_n$, $n=0-5$, obtained at 355 nm. All images were acquired under similar experimental conditions and are shown to scale. Double arrow in the $n=0$ image indicates the direction of the laser polarization for all images. The $n=0$ image is the same as in Fig. 1(c), shown here on a different scale.

spectrum is related to the strength of the ion-solvent interaction, where anionic geometries caused by stronger ionic H bonds lead to higher vibrational excitations in the resulting neutral complex. In addition, Myshakin *et al.*[34] found two isomeric species for $NO^-(H_2O)_n$, with the H bonds forming with either the N or O atom of the NO^- core, contributing to additional line broadening.

B. Photoelectron angular distributions for unsolvated NO^-

The PADs resulting from one-photon detachment with linearly polarized light are generally described as $I(\theta) \propto 1 + \beta P_2(\cos\theta)$, where β is the anisotropy parameter, θ is the angle between the photoelectron velocity and the laser polarization vectors, and P_2 is the second-order Legendre polynomial.[35,36] Inspection of Fig. 1 reveals a perpendicular ($\beta<0$) nature of the NO^- PADs. Negative β values are generally expected in the detachment from antibonding π orbitals of diatomic anions, as discussed, for example, in regard to π_g^{-1} photodetachment of O_2^- (Ref. 37) and S_2^-.[21] Although NO^- lacks inversion symmetry, its $2p\pi^*$ highest occupied molecular orbital (HOMO) (shown in the inset in Fig. 4) is qualitatively similar to O_2^- and the observed negative anisotropy is therefore not surprising.

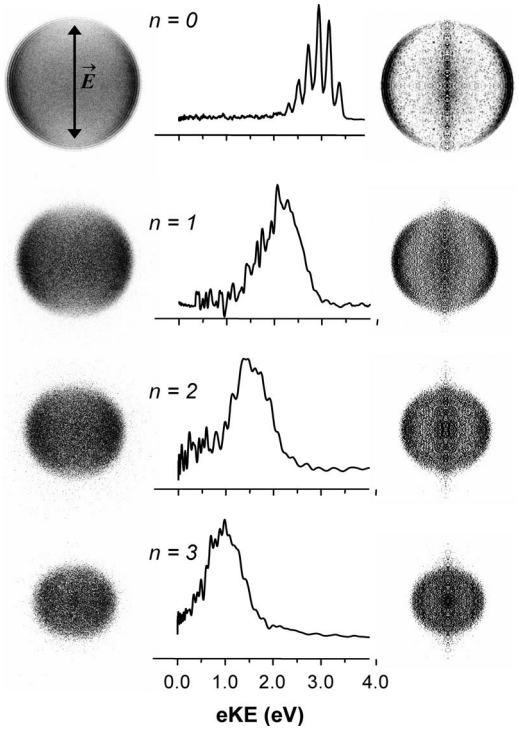

FIG. 3. Raw (left column) and Abel-inverted (right column) photoelectron images and corresponding spectra obtained at 355 nm for $NO^-(H_2O)_n$, $n=0-3$. All images were acquired under similar experimental conditions and are shown to scale. Double arrow in the $n=0$ images indicates the direction of the laser polarization for all images. The $n=0$ image is the same as in Fig. 1(c), shown here on a different scale.

The β values for the individual vibrationally resolved rings in the 786, 532, and 355 nm NO^- photoelectron images (Fig. 1) are plotted versus the corresponding eKE values in Fig. 4 (gray open circles). The results for each wavelength appear to follow parabolic patterns, consistent between multiple experimental runs on two different instruments in our laboratory. The patterns are indicated by dashed parabolas in Fig. 4, fitted to the corresponding data; however, this intriguing observation falls outside the scope of this report. Averaged β values (corresponding to the PADs integrated over the entire Franck-Condon envelope of the transition) are shown in Fig. 4 as black filled circles. In addition, the averaged β value from a 266 nm NO^- photoelectron image[28] is included at average eKE=4.11 eV, as well as the vibrationally resolved 488 nm results of Siegel *et al.*, indicated by crosses.[26]

The β values in Fig. 4 are compared to a solid curve obtained by a nonlinear fit to the data using the Cooper-Zare central-potential model.[35,36] We used the simplified version of the model proposed by Hanstorp *et al.*,[38] which assumes no interaction between the departing electron and the neutral residue. The fitting procedure is described in the previous work.[8] Similar to the studies of S_2^- and O_2^-,[21,37,39] the $2p\pi^*$

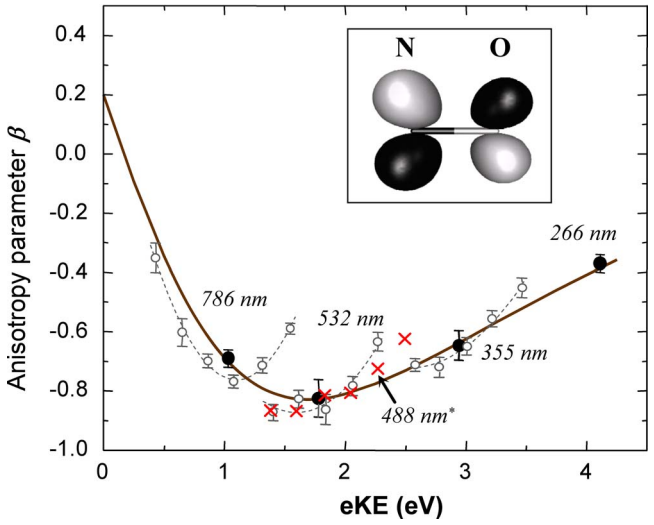

FIG. 4. (Color online) Gray open circles: the anisotropy parameter (β) values determined for vibrationally resolved NO^- photodetachment transitions at 786, 532, and 355 nm, corresponding to the photoelectron images in Figs. 1(a)–1(c), respectively. Dashed gray curves are parabolic fits to the vibrationally resolved data for each of the above wavelengths. Black filled circles: average β values obtained by integrating the 786, 532, 355, and 266 nm NO^- PADs over the entire Franck-Condon envelopes of the corresponding transitions, plotted as function of average eKE. Red crosses: vibrationally resolved 488 nm β values from Ref. 26. Solid curve: the Cooper-Zare model fit to the average β data points (filled circles) obtained as described in the text. Inset shows a calculated isosurface plot of the $2p\pi^*$ orbital of NO^-.

HOMO of NO^- is approximated as a d-like orbital with an effective angular momentum quantum number $\ell=2$. For consistent comparison with the cluster data, only the average β values, corresponding to the integrated PADs (filled circles in Fig. 4), were used for the model fit. The resulting Cooper-Zare curve shown in Fig. 4 corresponds to $\cos\phi=0.881$ for the relative phase ϕ of the $\ell'=\ell\pm1$ partial waves and $A=0.383\ \mathrm{eV}^{-1}$ for the coefficient related to the spatial extent of the negative ion[38] [see Eq. (2) in Ref. 8].

C. Solvation effects on photoelectron anisotropy

The $NO^-(N_2O)_n$ PADs extracted from the images in Fig. 2 reveal a gradual loss of photodetachment anisotropy with increasing solvation. The trend is particularly notable in comparison with the PADs obtained for the $NO^-(H_2O)_n$ images in Fig. 3. The latter retain a greater degree of anisotropy upon hydration, despite the much larger spectral shifts induced by sequential addition of H_2O, compared to N_2O. This becomes particularly clear by direct comparison of the anisotropy parameter values obtained for the individual cluster ions by integrating the PADs over the corresponding spectral profiles. The resulting β values are plotted in Fig. 5(a) versus average eKE, which is used both as a measure of solvation and as a natural variable for comparison with the Cooper-Zare model. Four separate data sets are shown. Sets 1, 2, and 3, as labeled in Fig. 5, correspond to the $NO^-(N_2O)_n$ cluster anions studied at 355, 532, and 786 nm, respectively. The cluster sizes, indicated in Fig. 5(a) next to the data points, range from $n=0$ [unsolvated NO^-, filled black circles in Fig. 5(a)] to $n=7$, 5, and 3 for sets 1, 2, and 3, respectively. Set 4 corresponds to $NO^-(H_2O)_n$, $n=0-3$ at 355 nm. The β(eKE)

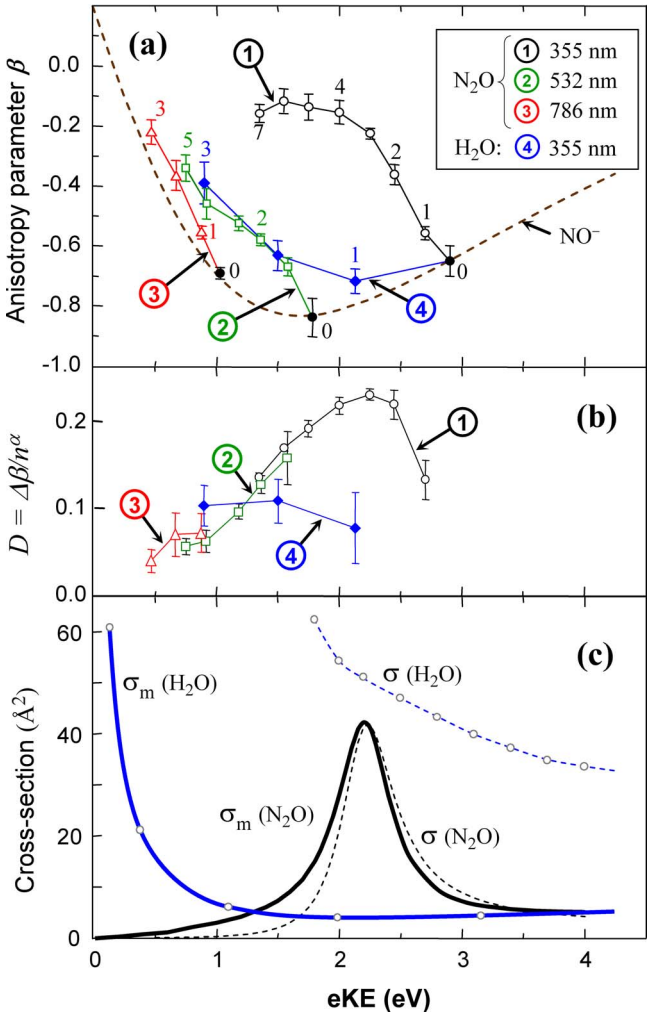

FIG. 5. (Color online) (a) Data series 1–4, as indicated in the legend: Photoelectron anisotropy parameters for $NO^-(N_2O)_n$ and $NO^-(H_2O)_n$ as functions of average eKE. The numbers of solvent molecules (n) are displayed next to the data points. The unsolvated NO^- ($n=0$) data, shown as filled circles, as well as the Cooper-Zare curve for bare NO^-, shown as a dashed line, are reproduced from Fig. 4. (b) Normalized anisotropy differential D (defined in the text) for data sets 1–4 from (a). (c) The absolute total cross section (dashed) and momentum-transfer cross section (solid) for electron collisions with N_2O (black) and H_2O (blue). The H_2O and N_2O cross section data are from Refs. 41 and 16, respectively.

trends are compared to the Cooper-Zare curve for unsolvated NO^-, determined in Fig. 4 and reproduced as a dashed curve in Fig. 5(a). The greatest deviation from the model prediction is exhibited by set 1, corresponding to $NO^-(N_2O)_n$ at 355 nm.

To quantify the deviations in β and account for the varying number of solvent molecules n, we introduce a normalized solvent-induced anisotropy differential D defined as

$$D=\Delta\beta/n^{\alpha}, \tag{1}$$

where $\Delta\beta=\beta(\mathrm{eKE})-\beta_{CZ}(\mathrm{eKE})$, with β(eKE) and β_{CZ}(eKE) being the $n>0$ data from Fig. 5(a) and the $n=0$ Cooper-Zare predicted values, respectively, and α is an empirical exponent. Thus defined, D is not intended as a rigorous measure of solvation effects. It is proposed only for clarifying the observed trends and discriminating between the factors in play, namely, the eKE dependence and solvent coordination.

Subtracting β_{CZ}(eKE) in $\Delta\beta$ accounts for the expected Cooper-Zare model trend, as applied to the (unperturbed) core NO^- anion photodetachment, with the balance attributed to the solvent effects. These are expected to depend on the solvent nature and the number of solvent molecules present. Since the scaling of $\Delta\beta$ with n is unlikely to be linear, an empirical n^α normalization is included in Eq. (1), with α expected to be between 0 and 1.

The four sets of D values, corresponding to sets 1–4 defined above ($n>0$), are plotted in Fig. 5(b) using $\alpha=0.8$. This empirical value is chosen arbitrarily to match the D values for sets 1 and 2 and 2 and 3 within the overlapping eKE ranges; however, reasonable variations in α do not change the foregoing conclusions. The resulting D(eKE) variations for sets 1–3, on the one hand, and set 4, on the other, represent the energy-dependent effects on the PADs attributed to the solvation by N_2O and H_2O, respectively, normalized (empirically) to the numbers of solvent molecules in the corresponding clusters.

IV. DISCUSSION

Viewing cluster photodetachment as electron ejection from the core anion, followed by its scattering on the solvent, the PADs can be affected by the solvent via the following mechanisms. First is the change in the partial-wave balance due to the solvation-induced decrease in eKE. Second is the solvent-induced perturbation of the initial electronic state, including any distortions of the core-anion geometry and/or symmetry, as well as possible delocalization of the excess electron to the solvent. Third is the departing electron scattering on the solvent molecules.

In our analysis, the first of the above effects is accounted for by comparing the observed anisotropy values to the Cooper-Zare model predictions. Regarding the second, only minimal distortion of the core-anion structure and/or charge delocalization to the solvent network is indicated in Figs. 2 and 3, where the cluster anion spectra clearly retain the NO^- character. In addition, *ab initio* calculations on $NO^-\cdot N_2O$ predicted only a 2% charge delocalization to the solvent molecule.[40] This brings our focus to electron scattering on the solvent.

Shown as dashed curves in Fig. 5(c) are the total electron scattering cross sections, σ(eKE), for N_2O and H_2O, based on the data from Refs. 16 and 41, respectively. The N_2O+e^- cross section reveals a resonance with a maximum at 2.25 eV. In contrast, the H_2O+e^- curve reflects a steep decline with increasing eKE in the low-eKE region, with no evidence of resonances in the region of interest. Nonetheless, the total cross section for H_2O *exceeds* that for N_2O in the entire range shown. This seemingly contradicts our principal conclusion ascribing the anisotropy decay in cluster anion photodetachment primarily to electron-solvent scattering.

To reconcile these observations, we consider the qualitatively different electron scattering mechanisms for H_2O and N_2O. The H_2O+e^- scattering in the 0–4 eV range is dominated by long-range interaction of the electrons with the molecular dipole moment. Classically speaking, most scattering events occur with large impact parameters and lead to small-angle scattering of the incident electrons. This expectation is confirmed by the dependence of the H_2O+e^- differential cross section $\sigma_{diff}(\theta_e,\text{eKE})$ on the scattering angle θ_e, which peaks very strongly in the forward direction (i.e., near $\theta_e=0°$).[41,42] Specifically, in the vicinity of 2 eV, the differential cross section for H_2O+e^- forward scattering is estimated to exceed that for backward scattering ($\theta_e=180°$) by about two orders of magnitude (Fig. 1 in Ref. 42). In other words, the trajectories of most electrons scattered by H_2O are affected rather little.

In contrast, the N_2O+e^- scattering dynamics in the same energy range are dominated by the $^2\Pi$ symmetry N_2O^- resonance.[18] One might think of the resonance as an absorber, which reemits the scattered electrons in varying directions, subject to the conservation of energy and angular momentum.[17] Accordingly, the N_2O+e^- differential cross section shows nearly equal probabilities for forward and backward scattering near the resonance maximum [Fig. 3(a) in Ref. 16]. Hence, the electron trajectories get scrambled by the interaction with N_2O in the vicinity of the anionic resonance.

These scattering features align well with the stronger decay of photodetachment anisotropy observed with N_2O solvation, despite the larger total cross section of H_2O. Furthermore, we conclude that the total scattering cross section is not necessarily a good measure for evaluating the solvent effects on the PADs in cluster anion photodetachment. Obtained by integrating the differential cross section over all scattering angles, σ(eKE) does not reflect the most relevant details of the interaction between the emitted electrons and the solvent molecules. A more appropriate measure is the momentum-transfer (or "diffusion") cross section σ_m(eKE), calculated by integrating $\sigma_{diff}(\theta_e,\text{eKE})$ with a $(1-\cos\theta_e)$ weight function.[15] The σ_m(eKE) cross section assigns a greater weight to scattering events that significantly alter the electron trajectories (and thus affect the PAD) and discounts small-angle scattering contributions.

The momentum-transfer cross sections for electron collisions with H_2O and N_2O are plotted as solid curves in Fig. 5(c), using the results of Refs. 41 and 16, respectively. For N_2O, σ_m(eKE) is not very different from the corresponding total cross section, implicating that most N_2O+e^- collisions in the relevant energy range are "momentum-transfer" collisions. For H_2O+e^-, however, σ_m is reduced by orders of magnitude relative to σ, as most scattering events are long-range electron-dipole interactions, not causing significant changes to the electron trajectories.

The normalized anisotropy differentials for the N_2O and H_2O solvents, shown in Fig. 5(b), mirror the main trends of the corresponding momentum-transfer cross sections in Fig. 5(c). For N_2O (sets 1–3), D(eKE) peaks near the $^2\Pi$ resonance maximum, while the less significant anisotropy loss in $NO^-(H_2O)_n$ is consistent with the smaller σ_m(eKE) values for H_2O. While the agreement is by no means quantitative, it does bring out the role of the N_2O^- resonance.

A major limitation of the above analysis is the empirical nature of Eq. (1). In addition, one must consider that electron-solvent scattering interactions in cluster anion photodetachment occur in the short range, while the measured

eKEs correspond to final (far-field) energies of the detached electrons. Assuming attractive electron-neutral interactions, the effective energy of the outgoing electrons in the solvent-scattering process is greater than the measured eKE, which should result in a redshift or redwing broadening of the scattering profile. This effect possibly contributes to the low-eKE slope of D(eKE) in Fig. 5(b), which extends beyond the unsolvated resonance curve. Resonance broadening by the cluster environment and collective many-body effects are also likely to contribute to the broadening of the D(eKE) curve.[43,44]

The suggested role of the N_2O^- resonance echoes with the past work on solvated iodide cluster anions, in which a marked loss of anisotropy with a single CH_3I solvent molecule implicated a CH_3I^- scattering resonance.[8] In general, we believe that in many cases the solvent-induced reduction of photoelectron anisotropy can be traced to a large electron-solvent momentum-transfer cross section, such as expected in the case of a resonance found in the outgoing photoelectron energy range. As one more case in point, a marked loss of photodetachment anisotropy upon solvation was previously observed by our group for the $(OCS)_n^-$ cluster anions. Although we did not explicitly comment on it at the time, the trend is clearly seen in the outer rings of the 400 nm photoelectron images of $(OCS)_n^-$ in Fig. 1 in Ref. 45. In that case, eKE falls in the vicinity of the $^2\Pi$ shape resonance of OCS peaking at 1.15 eV.[46] This example is particularly relevant here, because of the similarities between OCS and N_2O, including their structures and electron affinities.[47]

V. SUMMARY

Photoelectron images of solvated NO^- obtained at several laser wavelengths reveal a greater reduction in the photodetachment anisotropy in the presence of N_2O solvent molecules, compared to H_2O. The effect is attributed to an N_2O solvent anionic resonance that falls within the departing electron kinetic energy range. The momentum-transfer cross section, rather than the total scattering cross section, is shown to be a better predictor of the solvent effects on the photoelectron angular distributions in these cluster anions.

ACKNOWLEDGMENTS

We thank Professor J. Mathias Weber at JILA, the University of Colorado, Boulder, for helpful comments on this work. We are also grateful to Dr. Andreas Osterwalder and Professor Daniel M. Neumark (University of California, Berkeley) for technical help with event-counting imaging. This work is supported by NSF Grant No. CHE-0134631.

[1] A. W. Castleman and K. H. Bowen, J. Phys. Chem. **100**, 12911 (1996).
[2] A. Sanov and W. C. Lineberger, Phys. Chem. Chem. Phys. **6**, 2018 (2004).
[3] D. W. Chandler and P. L. Houston, J. Chem. Phys. **87**, 1445 (1987).
[4] A. T. J. B. Eppink and D. H. Parker, Rev. Sci. Instrum. **68**, 3477 (1997).
[5] R. Mabbs, E. Surber, and A. Sanov, Analyst (Cambridge, U.K.) **128**, 765 (2003).
[6] R. Mabbs, E. Surber, L. Velarde, and A. Sanov, J. Chem. Phys. **120**, 5148 (2004).
[7] L. G. Christophorou and J. K. Olthoff, *Fundamental Electron Interactions* (Kluwer Academic/Plenum, New York, 2004).
[8] R. Mabbs, E. Surber, and A. Sanov, J. Chem. Phys. **122**, 054308 (2005).
[9] R. Nakanishi, A. Muraoka, and T. Nagata, Chem. Phys. Lett. **427**, 56 (2006).
[10] J. V. Coe, J. T. Snodgrass, K. M. Friedhoff, and K. H. Bowen, J. Chem. Phys. **87**, 4302 (1987).
[11] J. H. Hendricks, H. L. de Clercq, C. B. Freidhoff, S. T. Arnold, J. G. Eaton, C. Fancher, S. A. Lyapustina, J. T. Snodgrass, and K. H. Bowen, J. Chem. Phys. **116**, 7926 (2002).
[12] M. S. Resat, V. Zengin, M. C. Garner, and R. E. Continetti, J. Phys. Chem. A **102**, 1719 (1998).
[13] M. M. Maricq, N. A. Tanguay, J. C. Obrien, S. M. Rodday, and E. Rinden, J. Chem. Phys. **90**, 3136 (1989).
[14] M. C. McCarthy, J. W. R. Allington, and K. S. Griffith, Chem. Phys. Lett. **289**, 156 (1998).
[15] *Electron-Molecule Collisions*, edited by I. Shimamura and K. Takahashi (Plenum, New York, 1984).
[16] C. Winstead and V. McKoy, Phys. Rev. A **57**, 3589 (1998).
[17] F. A. Gianturco and T. Stoecklin, Eur. Phys. J. D **40**, 369 (2006).
[18] M. Kitajima, Y. Sakamoto, R. J. Gulley, M. Hoshino, J. C. Gibson, H. Tanaka, and S. J. Buckman, J. Phys. B **33**, 1687 (2000).
[19] H. Hotop, M. W. Ruf, M. Allan, and I. I. Fabrikant, Adv. At., Mol., Opt. Phys. **49**, 85 (2003).
[20] J. M. Weber, E. Leber, M. W. Ruf, and H. Hotop, Phys. Rev. Lett. **82**, 516 (1999).
[21] E. Surber, R. Mabbs, and A. Sanov, J. Phys. Chem. A **107**, 8215 (2003).
[22] M. A. Johnson and W. C. Lineberger, in *Techniques for the Study of Ion Molecule Reactions*, edited by J. M. Farrar and W. H. Saunders (Wiley, New York, 1988), p. 591.
[23] L. A. Posey and M. A. Johnson, J. Chem. Phys. **88**, 5383 (1988).
[24] S. A. Chacko and P. G. Wenthold, Mass Spectrom. Rev. **25**, 112 (2006).
[25] M. J. Travers, D. C. Cowles, and G. B. Ellison, Chem. Phys. Lett. **164**, 449 (1989).
[26] M. W. Siegel, R. A. Bennett, R. J. Celotta, J. L. Hall, and J. Levine, Phys. Rev. A **6**, 607 (1972).
[27] V. Dribinski, A. Ossadtchi, V. A. Mandelshtam, and H. Reisler, Rev. Sci. Instrum. **73**, 2634 (2002).
[28] L. Velarde, Ph.D. thesis, University of Arizona, 2007.
[29] K. Hiraoka, S. Fujimaki, K. Aruga, and S. Yamabe, J. Phys. Chem. **98**, 8295 (1994).
[30] J. W. Torchia, K. O. Sullivan, and L. S. Sunderlin, J. Phys. Chem. A **103**, 11109 (1999).
[31] L. Velarde, T. Habteyes, and A. Sanov, J. Chem. Phys. **125**, 114303 (2006).
[32] A. Snis and I. Panas, Chem. Phys. Lett. **305**, 285 (1999).
[33] J. G. Eaton, S. T. Arnold, and K. H. Bowen, Int. J. Mass Spectrom. Ion Process. **102**, 303 (1990).
[34] E. M. Myshakin, K. D. Jordan, W. H. Robertson, G. H. Weddle, and M. A. Johnson, J. Chem. Phys. **118**, 4945 (2003).
[35] J. Cooper and R. N. Zare, J. Chem. Phys. **48**, 942 (1968).
[36] J. Cooper and R. N. Zare, J. Chem. Phys. **49**, 4252 (1968).
[37] F. A. Akin, L. K. Schirra, and A. Sanov, J. Phys. Chem. A **110**, 8031 (2006).
[38] D. Hanstorp, C. Bengtsson, and D. J. Larson, Phys. Rev. A **40**, 670 (1989).
[39] K. J. Reed, A. H. Zimmerman, H. C. Andersen, and J. I. Brauman, J. Chem. Phys. **64**, 1368 (1976).
[40] R. W. Góra, S. Roszak, and J. Leszczynski, Asian J. Spectrosc. **4**, 1 (2000).
[41] Y. Itikawa and N. Mason, J. Phys. Chem. Ref. Data **34**, 1 (2005).
[42] L. E. Machado, L. M. Brescansin, I. Iga, and M. T. Lee, Eur. Phys. J. D **33**, 193 (2005).
[43] C. E. Klots and R. N. Compton, J. Chem. Phys. **69**, 1636 (1978).
[44] G. Hanel, T. Fiegele, A. Stamatovic, and T. D. Mark, Int. J. Mass. Spectrom. **205**, 65 (2001).
[45] E. Surber and A. Sanov, J. Chem. Phys. **118**, 9192 (2003).
[46] C. Szmytkowski, G. Karwasz, and K. Maciag, Chem. Phys. Lett. **107**, 481 (1984).
[47] E. Surber, S. P. Ananthavel, and A. Sanov, J. Chem. Phys. **116**, 1920 (2002).